European Radiology (2019) 29:1986–1996
https://doi.org/10.1007/s00330-018-5704-8

NEURO

Radiomics based on multicontrast MRI can precisely differentiate among glioma subtypes and predict tumour-proliferative behaviour

Changliang Su[1] · Jingjing Jiang[1] · Shun Zhang[1] · Jingjing Shi[1] · Kaibin Xu[2,3] · Nanxi Shen[1] · Jiaxuan Zhang[1] · Li Li[1] · Lingyun Zhao[1] · Ju Zhang[1] · Yuanyuan Qin[1] · Yong Liu[2,3,4] · Wenzhen Zhu[1]

Received: 7 June 2018 / Revised: 27 July 2018 / Accepted: 3 August 2018 / Published online: 12 October 2018

Abstract

Purpose To explore the feasibility and diagnostic performance of radiomics based on anatomical, diffusion and perfusion MRI in differentiating among glioma subtypes and predicting tumour proliferation.

Methods 220 pathology-confirmed gliomas and ten contrasts were included in the retrospective analysis. After being registered to T2FLAIR images and resampling to 1 mm^3 isotropically, 431 radiomics features were extracted from each contrast map within a semi-automatic defined tumour volume. For single-contrast and the combination of all contrasts, correlations between the radiomics features and pathological biomarkers were revealed by partial correlation analysis, and multivariate models were built to identify the best predictive models with adjusted 0.632+ bootstrap AUC.

Results In univariate analysis, both non-wavelet and wavelet radiomics features were correlated significantly with tumour grade and the Ki-67 labelling index. The max R was 0.557 (p = 2.04E-14) in T_1C for tumour grade and 0.395 (p = 2.33E-07) in ADC for Ki-67. In the multivariate analysis, the combination of all-contrast radiomics features had the highest AUCs in both differentiating among glioma subtypes and predicting proliferation compared with those in single-contrast images. For low-/high-grade gliomas, the best AUC was 0.911. In differentiating among glioma subtypes, the best AUC was 0.896 for grades II–III, 0.997 for grades II–IV, and 0.881 for grades III–IV. In predicting proliferation levels, multicontrast features led to an AUC of 0.936.

Conclusion Multicontrast radiomics supplies complementary information on both geometric characters and molecular biological traits, which correlated significantly with tumour grade and proliferation. Combining all-contrast radiomics models might precisely predict glioma biological behaviour, which may be attributed to presurgical personal diagnosis.

Key Points

- *Multicontrast MRI radiomics features are significantly correlated with tumour grade and Ki-67 LI.*
- *Multimodality MRI provides independent but supplemental information in assessing glioma pathological behaviour.*
- *Combined multicontrast MRI radiomics can precisely predict glioma subtypes and proliferation levels.*

Keywords Radiomics · Glioma · Neoplasm grading · Cell proliferation · Magnetic resonance imaging

Electronic supplementary material The online version of this article (https://doi.org/10.1007/s00330-018-5704-8) contains supplementary material, which is available to authorized users.

✉ Yong Liu
yliu@nlpr.ia.ac.cn

✉ Wenzhen Zhu
zhuwenzhen8612@163.com

[1] Department of Radiology, Tongji Hospital, Tongji Medical College, Huazhong University of Science and Technology, No. 1095, JieFang Avenue, Wuhan, Hubei, China

[2] Brainnetome Center and National Laboratory of Pattern Recognition, Institute of Automation, Chinese Academy of Sciences, Beijing, China

[3] School of Artificial Intelligence, University of Chinese Academy of Sciences, Beijing, China

[4] Center for Excellence in Brain Science and Intelligence Technology, Institute of Automation, Chinese Academy of Sciences, Beijing, China

Abbreviations

ADC	Apparent diffusion coefficient
ASL	Arterial spin labelling imaging
CBF	Cerebral blood flow
DWI	Diffusion-weighted imaging
eADC	Exponential apparent diffusion coefficient
FLAIR	Fluid-attenuated inversion recovery
T_1C	Contrast-enhanced T_1-weighted images
T_2FSE	T_2-weighted fast-echo images
VOI	Volume of interest

Introduction

Glioma is the most common neuroepithelial tumour of the cerebral nervous system, and the prognoses of these lethal brain cancers differ among gliomas due to their various biological tissue types. Among the numerous reported biomarkers, histological grade and the Ki-67 labelling index (Ki-67 LI) are two vital biological behaviour biomarkers. Lower-grade gliomas (grade II and III gliomas) may respond differently to the therapeutic schedule [1–3], progressing to glioblastoma or remaining indolent for years. High-grade glioma patients have a poor prognosis [4], although treated with standardised regimens. Regarding proliferation biomarkers, Ki-67 nuclear antigen is present only in proliferating cells, making it a reliable avenue for rapidly evaluating the growth fraction of normal and abnormal cells [5]. The overexpression of Ki-67, as stated in numerous investigations, infers the poor progression-free survival and overall survival of glioma patients, regardless of lesion region and pathological type [6, 7]. Hence, predicting presurgical histological grades and Ki-67 LI with high accuracy may highlight tumour invasive growth patterns, which might allow for a precise evaluation of tumour biological behaviour and aid in clinical treatment decision making for the precise management of glioma patients.

Previous studies have demonstrated that diffusion- and perfusion-weighted MRI could offer supplemental diagnostic information concerning non-invasive predictions of glioma subtype and tumour proliferation [8–10]. In addition to the advantages of no gadolinium administration, these techniques could reflect the metabolism status of brain tumours at the molecular level [11, 12]. However, these studies usually include only few parameters related to a certain contrast in MRI images and may suffer from bias caused by the selection of regions of interest [9, 13].

Since the conception of radiomics proposed in 2012 [14], much attention has focused on its application in the management of malignant cancer [15–18]. With numerous advanced, quantitative, high-throughput features extracted from medical images in the whole tumour volume, radiomics concepts have been used to develop diagnostic, predictive and prognostic models to support the development of personalised medicine [16]. For example, radiomics has been widely reported in predicting lymph node metastasis of colorectal cancer [19], forecasting the lung metastases of soft-tissue sarcomas of the extremities [20] and interpreting the gene-expression patterns and prognoses of head and neck cancers [21]. Radiomics offers a powerful and crucial approach for capturing intratumoural heterogeneity via abundant features obtained from radiological image data, which can potentially meet the demands of individualised medicine [22]. Considering the heterogeneous nature of most cancers, combining multicontrast MRI and radiomics may be critically important for diagnosing and treating glioma.

To explore the diagnostic performance of radiomics based on multicontrast MRI in differentiating among glioma subtypes and proliferation-related molecular biological behaviour, we conducted a multicontrast MRI radiomics study including 220 patients by a semi-automatic volume of interest (VOI) extraction method. Predictive performances were obtained and compared between both single-contrast and all-contrast MRI.

Materials and methods

This retrospective study was approved by the institutional ethics committee of the hospital performing the study and followed the Declaration of Helsinki tenets. Examinations were performed after informed consent was obtained. All data were collected from October 2012 to April 2017.

Patients

MRI images were acquired using a 3.0-Tesla scanner Discovery MR750 (GE Healthcare) with a 32-channel head coil. To limit the potential effect of head motion, patients were instructed not to move their heads during the scan. Multicontrast MRI images, including anatomical, diffusion-weighted and perfusion-weighted images, were acquired. Each image modality consisted of several contrasts. For instance, the anatomical images included T2-weighted fast-echo images (T2FSE), T1-weighted and T2-weighted fluid-attenuated inversion recovery (FLAIR) images, and contrast-enhanced T_1-weighted images (T_1C). Diffusion-weighted imaging (DWI) was acquired with three diffusion-encoding directions and two b-values (b = 0 and b = 1,000 s/mm^2). Both the original diffusion-weighted images and reconstructed apparent diffusion coefficients (ADCs) and exponential apparent diffusion coefficient (eADC) maps were obtained in the following radiomics analysis. Perfusion-weighted imaging was performed using a pseudo-continuous arterial spin labelling (ASL) sequence resulting in perfusion-weighted images (PW map) and reference

images, as well as cerebral blood flow (CBF) maps. The main parameters of each sequence are listed in Supplementary Table 1. The Ki-67 LI was obtained using standard immunohistochemical staining procedures in the post-operation samples.

In total, 220 glioma patients were included, and detailed information regarding tumour grade and Ki-67 LI for each contrast is summarised in Supplementary Table 1. Among all patients, three cases were excluded for the diagnosis of glial cell hyperplasia, and there were five cases of grade I, 90 of grade II, 61 of grade III and 61 of grade IV glioma according to the 2007 WHO Classification of Tumours of the Central Nervous System [23]. According to the classification criteria of Beesley and Mclaren [24], Ki-67 LI was divided into four levels based on the percentage of positive staining: 0–5% for level 0, 6–25% for level 1, 26–50% for level 2 and < 50% for level 3. In this study, levels 0 and 1 were treated as positive levels, and levels 2 and 3 were regarded as highly positive levels.

Data preprocessing

The entire workflow of the analysis is briefly and precisely summarised in Fig. 1. Ten contrasts – ADC, eADC, CBF, PW map, b_{1000}, b_0, T1FLAIR, T2FLAIR, T2FSE and T_1C – were prepared, and the main detailed scanning parameters and corresponding demographical data are listed in Supplementary Table 1.

All images were co-registered to the T2FLAIR image for each subject through standard procedures in SPM8 (Wellcome Department of Imaging Neuroscience, London, UK; http://www.fil.ion.ucl.ac.uk/spm/software/spm8/). Specifically, images from the anatomical modality, such as T1FLAIR, T2FSE and T_1C images, were directly co-registered to T2FLAIR. For the diffusion modality, all metrics were co-registered to T2FLAIR images after eddy current correction in FSL (The Oxford Centre for Functional MRI of the Brain, London, UK; https://fsl.fmrib.ox.ac.uk/fsl/fslwiki/). Finally, the PW images were directly co-registered to T2FLAIR, while

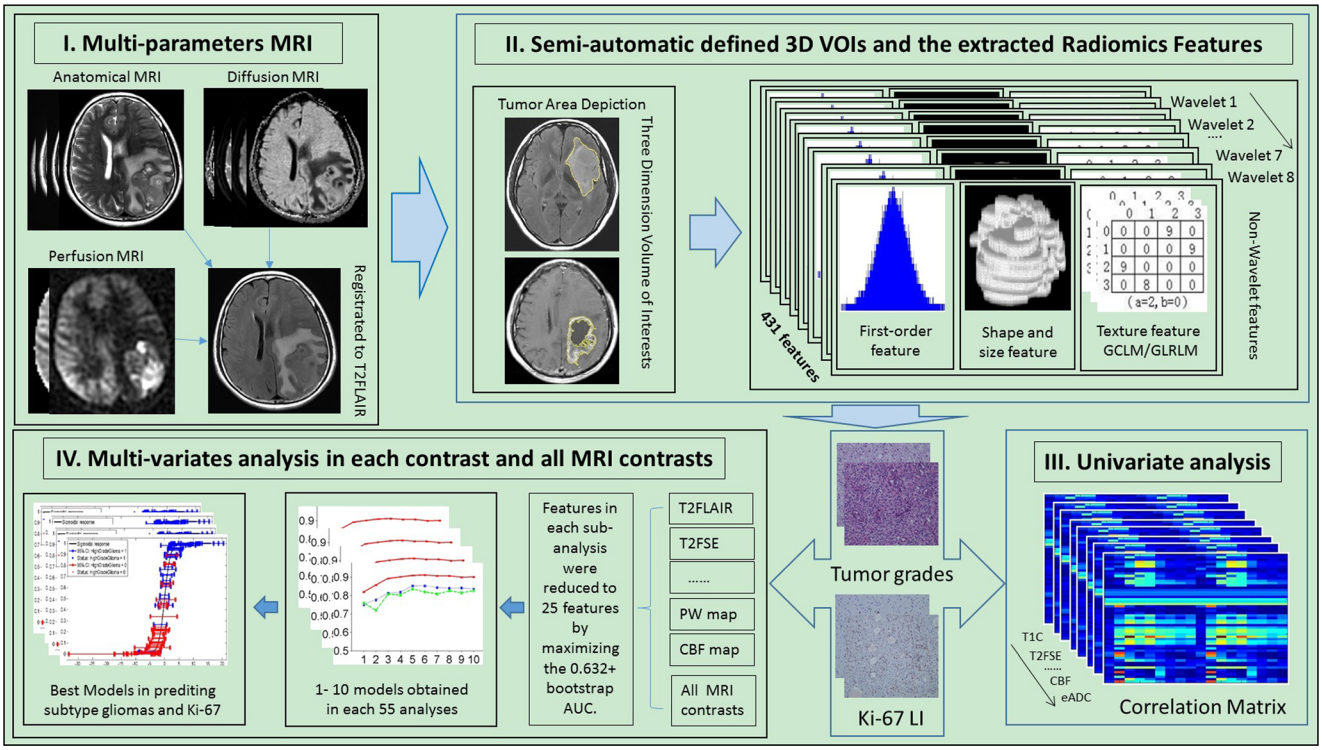

Fig. 1 Work flowchart of the entire study. **Step I. Multicontrast MRI preprocessing.** Multimodality MRI including anatomical MRI (T1FLAIR, T2FSE, T_1C, and T2FLAIR), diffusion-weighted MRI (B0, B1000, ADC and eADC) and perfusion-weighted MRI (PW and CBF). All images were registered to T2FLAIR and then resampled to 1 mm^3 isotropically. **Step II. Semi-automatic depicted VOIs and radiomics feature extraction.** VOIs were drawn by an experienced radiologist using the semi-automatic method based on the image signal threshold, and 431 radiomics features, including non-wavelet features and wavelet features (extracted after wavelet transformed with bandwidth 1–8), were extracted within VOIs. **Step III. Univariate analysis.** Radiomics features of ten included contrasts were correlated with histological grades and Ki-67 LI, and the correlations were precisely and visually displayed in correlation matrix maps. **Step IV. Multivariate analysis in single-contrast and all MRI contrasts.** The predictive performances of radiomics models were tested in subtype gliomas (grade II-III, II-IV, III-IV, and low/high grade glioma) and positive/highly positive Ki-67 LI, resulting in 55 sub-analyses. In each sub-analysis, the features were reduced to 25 features using 0.632+ AUC bootstrap, and 1–10 models were obtained. The final best models for predicting glioma subtypes and Ki-67 levels were obtained by comparing those in single MRI contrast or combining all contrasts

Table 1 Univariate results of radiomic features with glioma grade and Ki-67 LI

Part 1. Shape- and size-based features

Tumour grade	Features	Area	Volume	Compactness1	Compactness2	Max3dDiam	Spherical Disprop	Sphericity	Surf2VolRatio
	R	-0.046	-0.160	-0.199	-0.190	-0.118	0.254	-0.237	0.300
	p-value	0.5042	0.0198	0.0037	0.0055	0.0869	0.0002	0.0005	9.05E-06
Ki-67 LI	R	-0.097	-0.206	-0.248	-0.143	-0.143	0.172	-0.166	0.254
	p-value	0.2162	0.0080	0.0014	0.0668	0.0676	0.0279	0.0336	0.0010

Part 2. Non-shape and non-size features

	Tumour grade				Ki-67 LI			
Sequences	Max R	*p*-value	Feature number1[#]	Feature number2[##]	Max R	*p*-value	Feature number1[#]	Feature Number2[##]
ADC	0.353	1.75E-07	228	18	0.395	2.33E-07	227	1
CBF	0.269	3.06E-04	107	0	0.286	3.40E-04	162	0
PW	0.285	6.66E-08	154	1	0.293	1.05E-04	142	0
T_1C	0.557	2.04E-14	321	145	0.389	6.62E-06	275	6
T1FLAIR	0.425	3.78E-09	235	69	0.373	1.13E-05	193	1
T2FLAIR	0.342	1.94E-10	212	33	0.282	5.61E-05	204	0
T2FSE	0.429	2.23E-09	244	60	0.391	3.35E-06	212	1
b0	0.374	2.87E-08	246	61	0.338	1.05E-05	239	1
b1000	0.430	9.29E-11	313	94	0.367	1.75E-06	270	9
eADC	0.434	6.50E-11	303	103	0.369	1.60E-06	264	10

Nine features based on Shape and Size were separately correlated with tumour pathological biomarkers to avoid the repetitive correlation analysis in each contrast (Part 1). Surf2VolRatio showed the most significant correlation with tumour grade and Ki-67 LI. The correlation results for non-shape and non-size features were concisely concluded in Part 2. The maximum correlation coefficients, minimum *p*-value, number of *p*-values less than 0.05 (uncorrected) and number of *p*-values less than the Bonferroni correction *p*-value ($p_{corrected}$ = 1.16e - 05) are summarised in Part 2 for each contrast

represents the number of *p*-values < 0.05 (uncorrected)

represents the number of *p*-values less than the Bonferroni correction *p*-value ($p_{corrected}$ = 1.16e - 05)

the CBF maps were co-registered via PW maps. After registration, all maps were resampled to 1 mm^3.

Definition of the volume of interest

To define the solid parts of the tumours, both anatomical images and b_{1000} maps were used to delineate the regions of interest (ROIs). The volumes of interest (VOIs) were drawn by an experienced radiologist (4 years of experience) using semi-automatic methods as described previously [25], and representative cases for VOIs are displayed in Supplementary Fig. 1. Necrotic, cystic and oedema areas were carefully avoided to minimise mistaking them for the tumour parenchyma. The drawn VOIs were then saved as masks for all images to extract radiomics features.

Radiomics features

For each modality, radiomics feature extraction was conducted as previously described [21] to quantitatively describe tumour characteristics, and each feature is defined in the Supplemental materials. These features were generally sorted into four groups: (i) first-order statistics features based on tumour intensity (n = 14); (ii) non-texture features based on shape and size (n = 8); (iii) texture features (n = 33); and (iv) wavelet features [n = (first-order statistics features + texture features) × 8]. Thus, 431 features were obtained. All calculation procedures were performed using the MATLAB platform.

Statistical analysis

To understand the correlations between the radiomics features extracted from each contrast with tumour grade and Ki-67 LI, partial correlation analysis was applied in a univariate analysis, and patients' age and sex were treated as control variables. The correlation analyses were conducted for each contrast, retrospectively.

In the multivariate analysis, an imbalanced-adjusted logistic regression developed by Vallières and colleagues [20] was employed to build the prediction models based on radiomics features in each contrast MR image and the combination of all MRI contrasts. For each classification model, the included dataset was reduced to 25 features using 1,000 bootstrap training samples. Next, models combining one to ten radiomics features were selected by maximising the area under the

receiver-operating characteristic curve (AUC) $_{632+}$ metric [26] within 1,000 bootstrap training and testing samples [26]. Finally, models with the best predictive properties were accepted as the final models, and AUCs, sensitivities and specificities were separately calculated.

Results

Univariate analysis

Radiomics features are significantly correlated with glioma grade

Concerning the shape- and size-based features, Volume, Compactness1, Compactness2, SphericalDisprop, Sphericity and Surf2Volume correlated significantly with tumour grade ($p < 0.05$, uncorrected), and the results are summarised in Table 1 (part 1). As displayed in Fig. 2, features from different contrast images were correlated with tumour grade based on their own characteristics. Among these contrasts, T_1C showed the best performance, and the PW and CBF maps showed relatively poor correlations with tumour grade, in accord with the statistical details listed in Table 1 (part 2).

Radiomics features are significantly correlated with Ki-67 LI

Regarding the shape- and size-based features, Volume, Compactness1, SphericalDisprop, Sphericity and Surf2Volume possessed significant correlations with tumour type ($p < 0.05$, uncorrected), as observed for tumour grade and in the statistical data (Table 1, part 1). As shown in Fig. 2, features from DWI and its related parameters correlated more strongly with Ki-67 LI than did other modalities, and perfusion-weighted images and CBF exhibited relatively weaker correlations with Ki-67 LI (Table 2, part 2).

Multivariate analysis

To explore the performance of radiomics features in separating tumour grades, multivariate analysis was implemented [20]. Different MRI contrasts varied their classification performances in grading gliomas and predicting tumour proliferation levels, and the AUCs, sensitivity and specificity of the combined radiomics feature models for each sub-analysis are listed in Table 2 for each contrast. Multicontrast radiomics features allowed for the precise prediction of tumour pathological features, and the integrated models with the best predictive performances are presented in Table 3 for each sub-analysis. The best predictive combinations of the multicontrast radiomics features from models 1–10 and their classification effects are displayed in Figs. 3 and 4.

Tumour grading

In differentiating between low- and high-grade gliomas, the AUCs were approximately 0.750 in CBF maps (sensitivity: 71.4%, specificity: 63.9%) and 0.846 in T_1C (sensitivity: 75.9%, specificity: and 77.9%) in the single-MRI sequence analysis. When the features from all contrasts of images were combined, multicontrast MRI exhibited excellent performance in differentiating between low- and high-grade gliomas (AUC: 0.911; sensitivity: 85.2%; specificity: 85%) (Table 2, Fig. 4a and b).

To further investigate radiomics features in classifying subtype gliomas, inter-grade multivariate analysis results were obtained. The identical sequence may represent a reverse manifestation in the classification of different tumour subtypes (Table 2). In each single-MRI contrast differentiating between grade II and grade III, the best AUC was observed in T2FSE (AUC: 0.819; sensitivity: 71.5%; specificity: 74.5%). The worst performance was observed in T1FLAIR images (AUC: 0.692; sensitivity: 58%; specificity: 70.2%). The combination of all-contrast MR images resulted in an AUC of 0.896 and obviously improved sensitivity (78.1%) and specificity (78.8%) (Table 2, Fig. 3a and b).

Regarding grade II and grade IV gliomas, all MRI sequences exhibited good diagnostic performance, and all AUC values exceeded 0.8. The lowest AUC value of 0.813 was found in the CBF map (sensitivity: 69.4%; specificity: 74.7%), and the highest AUC value of 0.929 was found in T_1C (sensitivity: 83.3%; specificity: 85.6%). In the combined radiomics features from all-contrast images, the AUC was 0.997 (sensitivity: 97.6%; specificity: 97.6%) (Table 2, Fig. 3c and d).

The AUCs of single-MRI contrast in predicting grade III and grade IV gliomas ranged from 0.712 to 0.811. The smallest AUC was evident in the b0 maps (sensitivity: 63.6%; specificity: 70.4%). The largest AUC 0.811 was observed in T1FLAIR (sensitivity: 71.0%; specificity: 77.2%). The models combining all radiomics features resulted in the best performance (AUC: 0.881; sensitivity: 80.0%; specificity: 76.9%) (Table 2, Fig. 3e and f).

Tumour proliferation level

Similar to predicting tumour grade, radiomics features based on multicontrast imaging were combined to build models reflecting the levels of Ki-67 LI. In single-MRI contrast analysis, the b0 map offered the smallest AUC of 0.745 (sensitivity: 77.0%; specificity: 46.0%), and T2FLAIR manifested the largest AUC of 0.847 (sensitivity: 82.5%; specificity: 62.0%). The combination of the multicontrast MRI radiomics features led to the best predictive performance (AUC: 0.936; sensitivity: 80.0%; specificity: 87.6% separately) (Table 2, Fig. 4c and d).

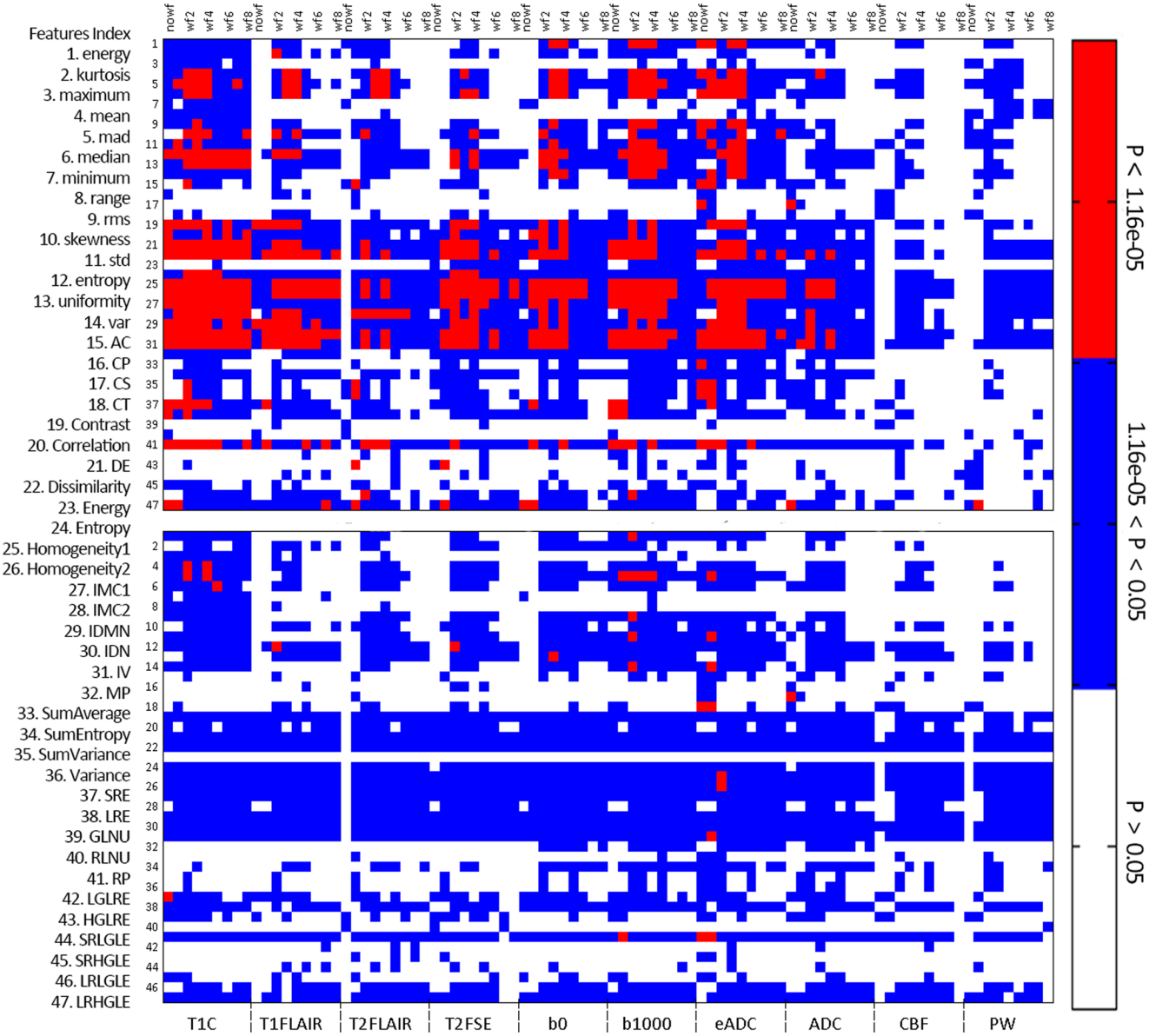

Fig. 2 Heat maps of the correlation *p*-value between non-shape-/size-based features and tumour grade and Ki-67 LI. The bottom X axis displays names of each contrast. The top X axis lists nine catalogues of radiomics features in each contrast. No-wf represents non-wavelet features, and Wf1-8 represents wavelet features based on wavelet bandwidths 1–8. The left Y axis shows radiomics feature names except for shape-/size-based features, and the detailed abbreviations are listed in the Supplementary materials. Red represents a *p*-value less than the Bonferroni-corrected *p*-value (1.16e - 05), and white represents a *p*-value greater than 0.05, while blue indicates a *p*-value for both. The heat map (upper) displays the distribution of the *p*-values obtained from the correlation analysis between multicontrast radiomics features with tumour grades. The heat map (bottom) displays the distribution of the *p*-values obtained from correlation analysis between multicontrast radiomics features with Ki-67 LI. Different correlation patterns can be clearly observed in each contrast

Discussion

This study demonstrated that radiomics features based on multicontrast MRI can supply independent but complementary information, which correlates significantly with glioma grade and Ki-67 LI. Moreover, models combining multicontrast MR radiomics features were built in a multivariate analysis, which could precisely predict glioma histological features and biological behaviour. These models might improve the prediction of glioma pathological behaviour and might be beneficial to the development of individualised medicine.

Multicontrast radiomics can precisely predict tumour pathological character

Analyses of a large amount of radiomics data revealed the significant correlations among multicontrast MRI radiomics

Table 2 Differentiation performance of multivariate models in sub-analysis

		ADC	CBF	PW	T_1C	T_1FLAIR	T_2FLAIR	T_2FSE	b_0	b_{1000}	eADC	Total
Grade II vs. III	AUC	0.81	0.72	0.74	0.76	0.69	0.77	0.82	0.76	0.75	0.77	0.90
	Sen	0.67	0.60	0.63	0.58	0.58	0.66	0.72	0.63	0.65	0.66	0.78
	Spec	0.75	0.68	0.70	0.80	0.70	0.73	0.74	0.74	0.72	0.72	0.79
Grade II vs. IV	AUC	0.87	0.81	0.84	0.93	0.85	0.92	0.91	0.84	0.86	0.88	0.99
	Sen	0.77	0.69	0.76	0.83	0.76	0.82	0.82	0.77	0.74	0.79	0.98
	Spec	0.77	0.75	0.74	0.86	0.81	0.84	0.84	0.80	0.79	0.83	0.98
Grade III vs. IV	AUC	0.74	0.80	0.79	0.74	0.81	0.75	0.77	0.71	0.76	0.78	0.88
	Sen	0.69	0.76	0.69	0.71	0.71	0.68	0.68	0.64	0.62	0.67	0.80
	Spec	0.65	0.70	0.72	0.65	0.77	0.71	0.70	0.70	0.72	0.72	0.77
Low-high grades	AUC	0.82	0.75	0.76	0.85	0.78	0.82	0.84	0.76	0.82	0.82	0.91
	Sen	0.76	0.71	0.73	0.76	0.75	0.77	0.79	0.74	0.72	0.76	0.85
	Spec	0.71	0.64	0.69	0.78	0.67	0.75	0.75	0.67	0.73	0.67	0.82
Positive and highly positive Ki-67 LI	AUC	0.82	0.83	0.82	0.82	0.76	0.85	0.77	0.75	0.80	0.80	0.94
	Sen	0.81	0.82	0.81	0.81	0.79	0.83	0.77	0.77	0.79	0.78	0.80
	Spec	0.64	0.55	0.55	0.60	0.42	0.62	0.48	0.46	0.55	0.54	0.88

For each sub-analysis, differentiations of the glioma subtypes (Grade II vs. III, Grade II vs. IV, and Grade III vs. IV) and Ki-67 LI levels (positive vs. highly positive) were performed within the combinations of radiomics features from single contrast and all contrasts. The AUCs, sensitivities and specificities are listed in the tables. Models obtained by combining all multicontrast radiomics features manifested the best predictive performance in each sub-analysis. "Sen" represents sensitivity, and "Spec" represents specificity (The smallest number of significant digits of the last two numbers was not two)

features with pathological biomarkers, and effective and non-invasive predictive models were built to classify different glioma subtypes and predict proliferation levels. As reported in a recent study [27], a relatively high predictive accuracy in distinguishing between grade II and III gliomas can be obtained using only conventional MRI sequences, partly agreeing with our results. However, compared with conventional MRI, functional MRI sequences can noninvasively provide supplementary quantitative biomarkers closely reflecting tumour pathological processes. The diffusion modality measures the water diffusion of tumour tissue, and its signal intensities reflect the restricted diffusion status, indicating the tumour cell density in lesions [28, 29]. Moreover, the rapid growth of tumour cells accompanied by the augmentation of blood perfusion and perfusion-weighted MRI can map different perfusion states in low- and high-grade gliomas [30, 31].

Table 3 Best predictive performance models for each sub-analysis

Sub-analysis	β and X	β0
Grade II vs. III	β = [2.901; -31.2; -0.01166; -2.158; -28.88; 0.004227]; X = [T2FSE--wf1-skewness; PW--wf4-SRLGLE; T1FLAIR--wf1-HGLRE; eADC--non_wf-skewness; T2FLAIR--wf2-IMC2; T2FLAIR--wf1- HGLRE];	32.65.
Grade II vs. IV	β = [-0.08116; 101; 19.74; -6.571]; X = [T2FLAIR--wf1-median; T_1C--non_wf-IMC1; PW--wf1-SRLGLE; eADC--wf1-kurtosis];	91.85.
Grade III vs. IV	β = [-55.46; -0.0003968; 4.497; -0.0003204; 40.87; 14.13]; X = [T1FLAIR--non_wf-Homogeneity1; b0--wf4-LRHGLE; T2FLAIR--wf1-skewness; b0--wf1-ClusterProminence; b0--wf1-Correlation; PW--non_wf-SRLGLE];	8.046.
Low vs. high grade	β = [-0.004046; -10.87; 5.775; -1.24; -0.01203; 0.004149]; X = [ADC--wf1-SumVariance; b0--wf2-Correlation; PW--wf1-SRLGLE; eADC--wf1-kurtosis; T2FLAIR--wf1-median; T_1C--wf1-std];	16.75.
Positive vs. highly positive Ki-67 LI	β = [3.063; -70.86; 0.0103; 0.0001565; -0.01035; -0.03349]; X = [T_1C--wf1-LRLGLE; T1FLAIR--wf2-Correlation; T_1C--wf1-median; ADC--non_wf-ClusterProminence; T1FLAIR--wf2-range; T_1C--wf1-mad];	20.83.

The models were expressed as $g(x) = \beta * X + \beta 0$, where β is the vector of coefficients for each contained radiomics features and X is the vector containing features from multicontrast radiomics. β0 is the coefficient for the linear logistic model. In the models obtained from each sub-analysis, multicontrast radiomics features, non-wavelet or wavelet features contribute to the highly accurate predictions of tumour pathological features

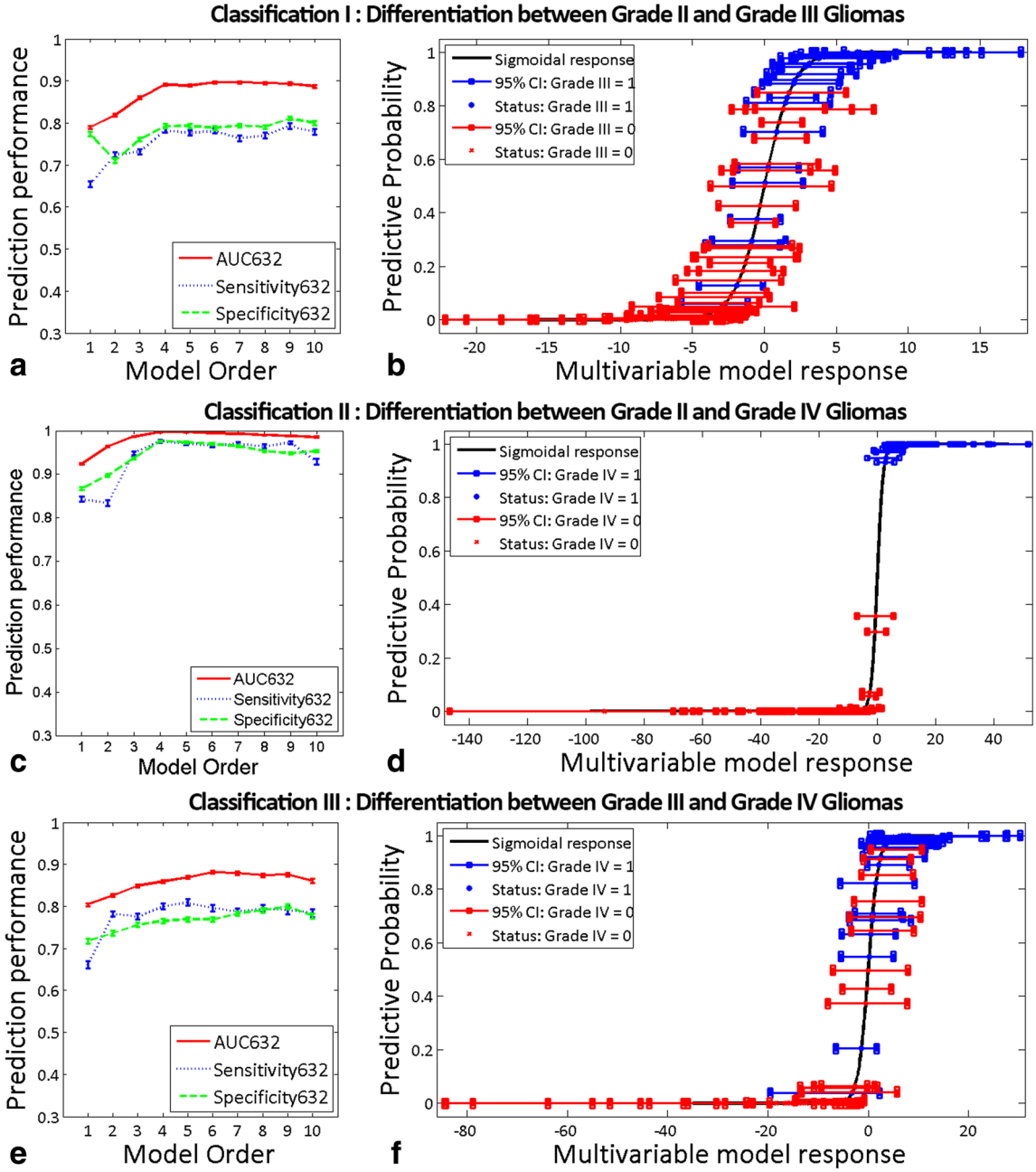

Fig. 3 Differentiating effect maps and models in differentiating between glioma subtypes. **a, b** Grade II-III gliomas; **c, d** grade II-IV gliomas; **e, f** grade III-IV gliomas. **a, c, e** Predictive performance of models 1–10 combining multicontrast radiomics features in predicting differentiating between subtypes of grade II vs. III, grade II vs. IV and grade III vs. IV. The AUCs, sensitivities and specificities are displayed for each model. **b, d, f** The sigmoid maps display the classification effects of the best predictive performance, in which higher-grade gliomas (**b, d, f**) are marked in blue, and their probabilities can be obtained at the left Y axis

Thus, diffusion- and perfusion-weighted MRI can provide supplemental information for depicting the heterogeneity of gliomas at different stages [32].

Conventional MRI, diffusion MRI and perfusion MRI reflect different aspects of gliomas, allowing for the prediction of glioma character with relatively high accuracy, as obtained in each contrast sub-analysis. However, the predictive performances of each contrast in differentiating the tumour subtypes and proliferation levels were unsatisfactory. Although the significance levels of the correlations between radiomics features based on PWI with pathological biomarkers were lower than those of other modalities in the univariate analyses, perfusion-related radiomics features were still integrated into the best predictive multivariate models. Combined analysis of all multicontrast radiomics features leads to a thorough and accurate understanding and evaluation of glioma biological behaviour and to distinct classification improvement compared with previous studies on glioma grading [27, 33, 34].

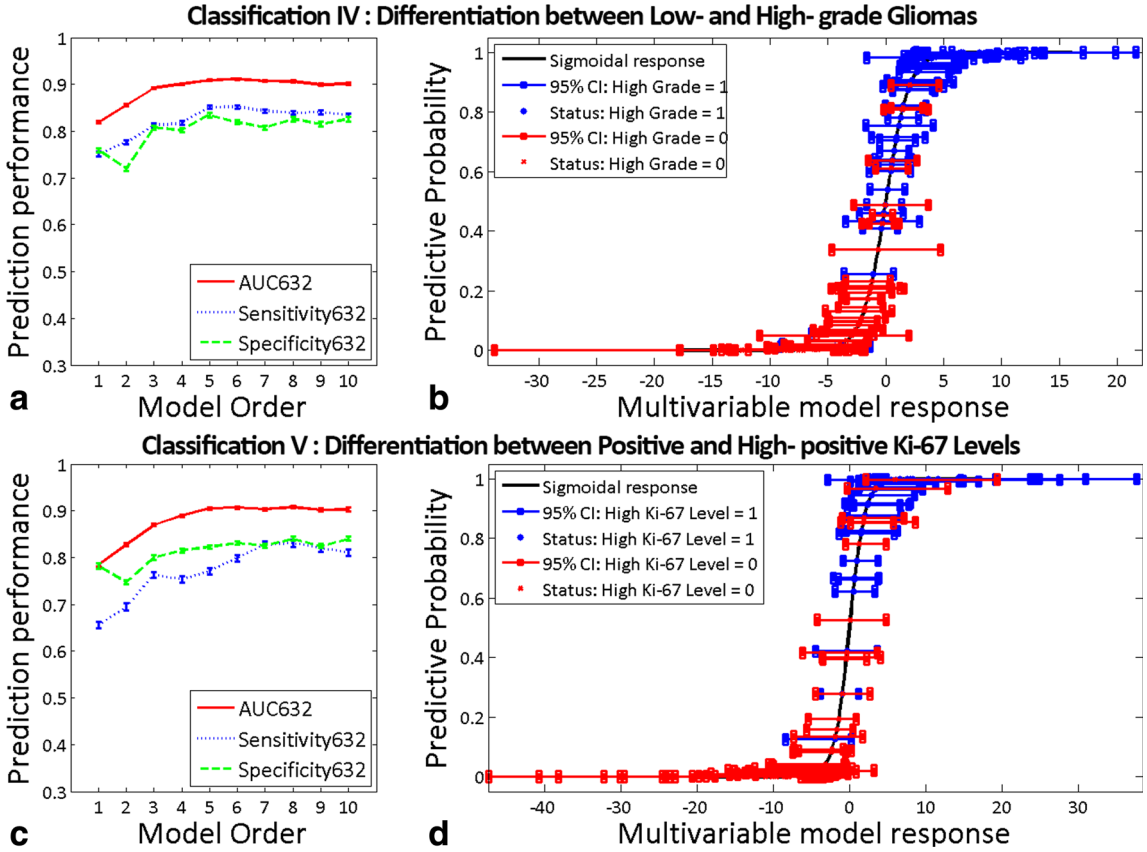

Fig. 4 Different effect maps and models in low-/high-grade gliomas and positive/highly positive Ki-67 LI. **a, b** Low-/high-grade gliomas; **c, d** positive/highly positive Ki-67 LI. **a, c** Predictive performance of models 1–10 combining multicontrast radiomics features in predicting low- and high-grade gliomas and in differentiating between positive and highly positive Ki-67 LI. The AUCs, sensitivities and specificities are displayed for each model. **b, d** The sigmoid maps display the classification effects of the best predictive performance, in which high-grade glioma (**b**) and highly positive Li-67 LI level (**d**) are marked in blue, and their probabilities can be obtained at the left Y axis

Radiomics features from different MR contrasts can supply distinctive but complementary information in reflecting tumour character, and those combinations allow for a comprehensive evaluation of glioma biological behaviour.

Multicontrast radiomics might serve as a vital tool for facilitating individualised medicine

Multicontrast MRI radiomics offers highly advanced quantitative features, and highly predictive models integrate these features and might facilitate the precise diagnosis of glioma patients. High-dimensional features related to shape and size, textural characteristics and properties [14] have been obtained and cannot be captured visually, the number of which is far greater than that reported in previous research based on only a few radiological features. These features allow for a more comprehensive assessment of distinct tumour heterogeneity with VOIs of whole lesions. Using machine learning methods, high-throughput features were reduced, selected and combined to build high-sensitivity and high-specificity predictive models [15, 35]. Although the diagnosis of glioma mainly depends on genetic mutation, for most patients diagnosed as a not otherwise specified (NOS) type, tumour grade and Ki-67 LI remain generally useful diagnostic and prognostic biomarkers. Our research provides evidence to support the application of non-invasive presurgery predicting two vital pathological biomarkers with multicontrast MRI radiomics. Given the relatively low cost of implementing MRI scanning and high accuracy in evaluating tumour subtypes, radiomics methods might provide relatively trustworthy values for presurgery treatment decisions, such as choosing craniotomy or biopsy for lesions and non-invasive preoperative grading evaluation.

The application of artificial intelligence in medicine is highly developed. As demonstrated by Zhang's team, artificial intelligence exhibited high accuracy and abilities equivalent to those of human experts in clinical diagnosis [18]. However, challenges persist, such as increased diagnostic certainty [36]. The models proposed in our research contain features from all included modalities, and both the non-wavelet features and wavelet-transformed features obtained improved classification performance in predicting glioma pathological behaviour. It is reasonable that multicontrast MRI might provide vital features to support the artificial intelligence system and thus

acquire more stable and robust clinical diagnostic decisions. Previous studies have proven that radiomics might be useful in predicting molecular characteristics and informing the targeted therapy and personalised treatment of gliomas [37, 38]. The combination of multicontrast MRI radiomics features will find its role in the precise management of glioma patients as a vital assisting tool and is worth looking into in the future.

Several limitations exist. First, although the predictive performances of multicontrast MRI radiomics features concerning glioma grade and proliferation were excellent, a possible shortage exists is the incompleteness of all the MR sequences in all the subjects. Moreover, due to the different slice thicknesses among ASLs with anatomical MRI and DWI, images were resampled to 1 mm^3 with interpolation, possibly producing bias in the quantitative calculation of radiomics features owing to a smoothing effect. Hence, the collection and evaluation of new glioma cases with high-resolution images is warranted. Additionally, our work may be partially recognised as a validation of the work of Zhou et al [27] regarding the differentiation of low-grade gliomas with conventional MRI radiomics. The models based on multicontrast radiomics obtained in our work remain to be validated regardless of their high predictive performance.

In conclusion, using univariate and multivariate analyses, we have provided reasonable evidence of radiomics based on multicontrast MRI in assessing glioma pathological behaviour. The features based on diverse modalities are significantly correlated with glioma pathological biomarkers. Disparate MRI modalities can provide distinctive but supplemental information, and thus, combined models can obviously enhance the accuracies of non-invasive presurgery glioma grading and evaluate tumour proliferation. Integrating geometric, signal and functional features based on multicontrast radiomics might meet the demands of an individual diagnosis and may serve a vital function in precision medicine.

Acknowledgements We acknowledge Dr. M Vallières for his patient responses regarding the radiomics data post-processing. We also acknowledge Dr. Yang Fan from General Electric Company (China) for his generous contributions to manuscript revision. We also thank Dr. Xiaowei Chen (10 years' experience) for his generous work in checking the VOIs.

Funding This study has received funding by the National Program of the Ministry of Science and Technology of China during the "12th Five-Year Plan" (ID: 2011BAI08B10) and the National Natural Science Foundation of China (No. 81171308, No. 81570462, and No. 81730049)

Compliance with ethical standards

Guarantor The scientific guarantor of this publication is Wenzhen Zhu.

Conflict of interest The authors of this manuscript declare no relationships with any companies whose products or services may be related to the subject matter of the article.

Statistics and biometry One of the authors has significant statistical expertise.

Informed consent Written informed consent was obtained from all subjects (patients) in this study.

Ethical approval Institutional Review Board approval was obtained.

Methodology
- Retrospective
- Observational
- Performed at one institution

References

1. van den Bent MJ (2014) Practice changing mature results of RTOG study 9802: another positive PCV trial makes adjuvant chemotherapy part of standard of care in low-grade glioma. Neuro Oncol 16: 1570–1574
2. van den Bent MJ, Wefel JS, Schiff D et al (2011) Response assessment in neuro-oncology (a report of the RANO group): assessment of outcome in trials of diffuse low-grade gliomas. Lancet Oncol 12: 583–593
3. Cancer Genome Atlas Research Network, Brat DJ, Verhaak RG et al (2015) Comprehensive, Integrative Genomic Analysis of Diffuse Lower-Grade Gliomas. N Engl J Med 372:2481–2498
4. Stupp R, Mason WP, van den Bent MJ et al (2005) Radiotherapy plus concomitant and adjuvant temozolomide for glioblastoma. N Engl J Med 352:987–996
5. Gerdes J, Lemke H, Baisch H, Wacker HH, Schwab U, Stein H (1984) Cell cycle analysis of a cell proliferation-associated human nuclear antigen defined by the monoclonal antibody Ki-67. J Immunol 133:1710–1715
6. Chen WJ, He DS, Tang RX, Ren FH, Chen G (2015) Ki-67 is a valuable prognostic factor in gliomas: evidence from a systematic review and meta-analysis. Asian Pac J Cancer Prev 16:411–420
7. Wakimoto H, Aoyagi M, Nakayama T et al (1996) Prognostic significance of Ki-67 labeling indices obtained using MIB-1 monoclonal antibody in patients with supratentorial astrocytomas. Cancer 77:373–380
8. Law M, Young R, Babb J et al (2006) Comparing perfusion metrics obtained from a single compartment versus pharmacokinetic modeling methods using dynamic susceptibility contrast-enhanced perfusion MR imaging with glioma grade. AJNR Am J Neuroradiol 27:1975–1982
9. Caulo M, Panara V, Tortora D et al (2014) Data-driven grading of brain gliomas: a multiparametric MR imaging study. Radiology 272:494–503
10. Inano R, Oishi N, Kunieda T et al (2014) Voxel-based clustered imaging by multiparameter diffusion tensor images for glioma grading. Neuroimage Clin 5:396–407
11. Krabbe K, Gideon P, Wagn P, Hansen U, Thomsen C, Madsen F (1997) MR diffusion imaging of human intracranial tumours. Neuroradiology 39:483–489
12. Garrett ME, Nauhaus I, Marshel JH, Callaway EM (2014) Topography and areal organization of mouse visual cortex. J Neurosci 34:12587–12600
13. Sui Y, Wang H, Liu G et al (2015) Differentiation of Low- and High-Grade Pediatric Brain Tumors with High b-Value Diffusion-weighted MR Imaging and a Fractional Order Calculus Model. Radiology 277:489–496
14. Kumar V, Gu Y, Basu S et al (2012) Radiomics: the process and the challenges. Magn Reson Imaging 30:1234–1248

15. Yip SS, Aerts HJ (2016) Applications and limitations of radiomics. Phys Med Biol 61:R150–R166
16. Avanzo M, Stancanello J, El Naqa I (2017) Beyond imaging: The promise of radiomics. Phys Med 38:122–139
17. Li Y, Liu X, Xu K et al (2018) MRI features can predict EGFR expression in lower grade gliomas: A voxel-based radiomic analysis. Eur Radiol 28:356–362
18. Kermany DS, Goldbaum M, Cai W et al (2018) Identifying Medical Diagnoses and Treatable Diseases by Image-Based Deep Learning. Cell Cell 172:1122–1131
19. Huang YQ, Liang CH, He L et al (2016) Development and Validation of a Radiomics Nomogram for Preoperative Prediction of Lymph Node Metastasis in Colorectal Cancer. J Clin Oncol 34: 2157–2164
20. Vallières M, Freeman CR, Skamene SR, El Naqa I (2015) A radiomics model from joint FDG-PET and MRI texture features for the prediction of lung metastases in soft-tissue sarcomas of the extremities. Phys Med Biol 60:5471–5496
21. Aerts HJ, Velazquez ER, Leijenaar RT et al (2014) Decoding tumour phenotype by noninvasive imaging using a quantitative radiomics approach. Nat Commun 5:4006
22. Gillies RJ, Kinahan PE, Hricak H (2016) Radiomics: Images Are More than Pictures, They Are Data. Radiology 278:563–577
23. Louis DN, Ohgaki H, Wiestler OD et al (2007) The 2007 WHO classification of tumours of the central nervous system. Acta Neuropathol 114:97–109
24. Beesley MF, McLaren KM (2002) Cytokeratin 19 and galectin-3 immunohistochemistry in the differential diagnosis of solitary thyroid nodules. Histopathology 41:236–243
25. Jiang R, Jiang J, Zhao L et al (2015) Diffusion kurtosis imaging can efficiently assess the glioma grade and cellular proliferation. Oncotarget 6:42380–42393
26. Sahiner B, Chan HP, Hadjiiski L (2008) Classifier performance estimation under the constraint of a finite sample size: resampling schemes applied to neural network classifiers. Neural Netw 21: 476–483
27. Zhou H, Vallières M, Bai HX et al (2017) MRI features predict survival and molecular markers in diffuse lower-grade gliomas. Neuro Oncol 19:862–870
28. Tien RD, Felsberg GJ, Friedman H, Brown M, MacFall J (1994) MR imaging of high-grade cerebral gliomas: value of diffusion-weighted echoplanar pulse sequences. AJR Am J Roentgenol 162:671–677
29. Lyng H, Haraldseth O, Rofstad EK (2000) Measurement of cell density and necrotic fraction in human melanoma xenografts by diffusion weighted magnetic resonance imaging. Magn Reson Med 43:828–836
30. Silva AC, Kim SG, Garwood M (2000) Imaging blood flow in brain tumors using arterial spin labeling. Magn Reson Med 44:169–173
31. Chawla S, Wang S, Wolf RL et al (2007) Arterial spin-labeling and MR spectroscopy in the differentiation of gliomas. AJNR Am J Neuroradiol 28:1683–1689
32. Kim HS, Kim SY (2007) A prospective study on the added value of pulsed arterial spin-labeling and apparent diffusion coefficients in the grading of gliomas. AJNR Am J Neuroradiol 28:1693–1699
33. Hwan-Ho C, Hyunjin P (2017) Classification of low-grade and high-grade glioma using multi-modal image radiomics features. 39th Annual International Conference of the IEEE Engineering in Medicine and Biology Society (EMBC), Seogwipo, 2017, pp. 3081–3084
34. Zhang X, Yan LF, Hu YC et al (2017) Optimizing a machine learning based glioma grading system using multi-parametric MRI histogram and texture features. Oncotarget 8:47816–47830
35. Lambin P, Rios-Velazquez E, Leijenaar R et al (2012) Radiomics: extracting more information from medical images using advanced feature analysis. Eur J Cancer 48:441–446
36. Thrall JH, Li X, Li Q et al (2018) Artificial Intelligence and Machine Learning in Radiology: Opportunities, Challenges, Pitfalls, and Criteria for Success. J Am Coll Radiol 15:504–508
37. Itakura H, Achrol AS, Mitchell LA et al (2015) Magnetic resonance image features identify glioblastoma phenotypic subtypes with distinct molecular pathway activities. Sci Transl Med 7:303ra138
38. Gevaert O, Mitchell LA, Achrol AS et al (2015) Glioblastoma Multiforme: Exploratory Radiogenomic Analysis by Using Quantitative Image Features. Radiology 276:313